Article

Effect of Al$_2$O$_3$ Content on High-Temperature Oxidation Resistance of Ti$_3$SiC$_2$/Al$_2$O$_3$

Yuhang Du [1], Qinggang Li [2,*], Sique Chen [2], Deli Ma [1], Baocai Pan [2], Zhenyu Zhang [1] and Jinkai Li [2]

1 Shandong Provincial Key Laboratory of Preparation and Measurement of Building Materials, Jinan 250022, China
2 School of Material Science and Engineering, University of Jinan, Jinan 250022, China
* Correspondence: mse_liqg@ujn.edu.cn

Abstract: Considering the lack of an effective anti-oxidation protective layer for the oxidation process of Ti$_3$SiC$_2$, an in situ synthesis of Ti$_3$SiC$_2$ and Al$_2$O$_3$ was designed. Thermally stable Al$_2$O$_3$ was used to improve the high-temperature oxidation resistance of Ti$_3$SiC$_2$. Samples without TiC were selected for the oxidation test, and the oxidation morphology and weight gain curves of the oxidized surface in air at 1400 °C are reported. The change in the oxidation behavior occurred 4 h after oxidation. The addition of Al$_2$O$_3$ changed the composition of the oxide layer and compensated for the lack of a dense protective layer during Ti$_3$SiC$_2$ oxidation. Moreover, after 4 h of oxidation, the newly generated Al$_2$TiO$_5$ and the composite layer formed by diffusion were the main reasons for the large difference in the final weight gain between the two sets of samples.

Keywords: Ti$_3$SiC$_2$; Al$_2$O$_3$; high temperature; oxidation resistance

1. Introduction

Ceramic is a type of material with unique characteristics, such as high-temperature oxidation resistance, high strength, and elastic stiffness, but it has inherent brittleness and low machinability [1–4]. A special group of materials in the ceramic family are the MAX-phase ceramics, which have a hexagonal structure and combined metal-ceramic properties. MAX-phase materials have broad application prospects owing to their excellent properties. However, compared with conventional ceramics, the hardness and high-temperature oxidation resistance of MAX-phase materials are lower, which significantly limits their application in the engineering field. Therefore, it is necessary to improve their mechanical properties and high-temperature stability. Ti$_3$SiC$_2$ is a MAX-phase compound with a layered structure that is a promising candidate for high-temperature applications [5,6]. In addition to its simple machinability, this material has excellent properties, such as electrical conductivity, thermal conductivity, and thermal shock resistance [7,8]. As a typical MAX-phase material, Ti$_3$SiC$_2$ is a promising structural ceramic for high-temperature applications such as heating elements in high-temperature furnaces and fuel-combustion components in automobiles and aircraft engines [9,10].

Notably, the oxidation resistance of Ti$_3$SiC$_2$ is crucial and has been investigated extensively, whether in the application of high-temperature structural ceramics or connection materials for solid oxide fuel cells. The preferential oxidation behavior of Ti$_3$AlC$_2$ is different from that of Ti$_3$SiC$_2$, which has a continuous Al$_2$O$_3$ layer [11–13]. The antioxidation capacities of Ti$_3$SiC$_2$ require further improvement for its effective application.

Reinforcement phases, including TiC, SiC, c-BN, TiB$_2$, and ZrO$_2$, have been used to improve the mechanical properties and oxidation resistance of Ti$_3$SiC$_2$ [14–17]. Li et al. [18] prepared dense SiC/Ti$_3$Si(Al)C$_2$ composites using an in situ hot-pressing sintering method and reported that the oxide layers formed at 1200 and 1300 °C were divided into outer, middle and inner layers. To obtain high-purity Ti$_3$SiC$_2$, Xu et al. [19] demonstrated that the incorporation of a small amount of Al was beneficial for improving the purity of Ti$_3$SiC$_2$.

Moreover, the addition of Al was advantageous for improving the oxidation resistance of the composites [20,21]. Some researchers believe that the optical and electrical properties of alumina at high temperature have crucial application value and prospects for fusion technology [22–24].

Thus, the dense Al_2O_3 layer formed during the oxidation of Ti_3AlC_2 is the design inspiration for this study. Moreover, considering the lack of an effective anti-oxidation protective layer in the Ti_3SiC_2 oxidation process, thermally stable Al_2O_3 is selected as a reinforcement phase in this study to change the oxidation resistance of Ti_3SiC_2. A Ti_3SiC_2/Al_2O_3 composite is synthesized in situ using the hot-pressing sintering method, and the high-temperature oxidation resistance of the composite is reported. Therefore, this study aims to present a detailed investigation of the high-temperature oxidation resistance of Ti_3SiC_2/Al_2O_3.

2. Experimental Procedure

The volume capacity of 30%, 40% and 50% Al_2O_3 were added and the powders of Ti:Si:TiC:Al in the molar ratio of 1:1.2:2:0.3 were used to synthesize Ti_3SiC_2/Al_2O_3 composites. In situ synthesis of Ti_3SiC_2 and Al_2O_3 was designed, namely TSC70 (Ti_3SiC_2/30 vol.% Al_2O_3), TSC60 (Ti_3SiC_2/40 vol.% Al_2O_3), TSC50(Ti_3SiC_2/50 vol.% Al_2O_3). TiC (99.9% purity, average particle size 1 µm, Shanghai ST-Nano Technology Co., Ltd., Shanghai, China), Ti (99.9% purity, average particle size 1–3 µm, Shanghai ST-Nano Technology Co., Ltd., Shanghai, China), Al (99.9% purity, average particle size 50 nm, Shanghai ST-Nano Technology Co., Ltd., Shanghai, China), Si (99.9% purity, average particle size 1 µm, Shanghai ST-Nano Technology Co., Ltd., Shanghai, China) and Al_2O_3 (99.9% purity, average particle size 30 nm, Shanghai ST-Nano Technology Co., Ltd., Shanghai, China) were used as raw materials. The original powders were mixed into ethanol by ball-milling for 4 h. Then the slurry was dried in a drying oven at 40 °C for 6 h and then sieved under 100 mesh. The Ti_3SiC_2/Al_2O_3 composites were in situ fabricated by vacuum hot-press sintering (VVPgr-80-2200, Shanghai, China) at 1450 °C with an applied pressure of 30 MPa for 1.5 h (the vacuum degree was 6.71×10^{-3} MPa).

For the oxidation experiments, rectangular blocks of size 5 mm × 4 mm × 4 mm were cut using a cylindrical SiC blade. The surface was polished with SiC paper. Thereafter, the samples were ultrasonically cleaned with ethanol to remove surface impurities. Oxidation tests was carried out in an alumina tube furnace at 1400 °C and the samples were exposed for up to 20 h. After the alumina tube furnace was heated to the test temperature, the block Ti_3SiC_2/Al_2O_3 composites to be tested were placed in the furnace. Using an electronic balance of accuracy 1×10^{-7} kg, the difference in weight gain was calculated.

X-ray diffraction (XRD) (D8 ADVANCE, Bruker, Saarbrucken, Germany) was used to confirm the phases of the samples before and after oxidation. The microstructure of the oxidized samples was observed by scanning electron microscopy (SEM) (FEI QUANTA FEG 250, Hillsboro, OR, USA) with energy dispersive X-ray spectrum (EDS).

3. Results and Discussion

The phase components of the Ti_3SiC_2/Al_2O_3 composite were characterized by X-ray diffraction (XRD). Figure 1 shows the XRD patterns of TSC70, TSC60 and TSC50 before oxidation. As shown in Figure 1, Ti_3SiC_2 and Al_2O_3 did not generate Ti–Al compounds, indicating that the composite degree between Ti_3SiC_2 and Al_2O_3 was appropriate. This plays an important role in the subsequent investigation of the high-temperature oxidation resistance of the Ti_3SiC_2/Al_2O_3 composite. Notably, several TiC peaks were observed in TSC70, but none were detected in TSC50 and TSC60. Under the same sintering conditions, the peak intensities of Al_2O_3 increased with increasing Al_2O_3 content, corresponding with the change in the volumetric fraction added during synthesis. This phenomenon indicates that the selection of the raw material was successful. Sun et al. [25] reported that the oxidation rate of Ti_3SiC_2 is slower than that of TiC, and TiC is detrimental to the oxidation

resistance of Ti_3SiC_2. Therefore, in the subsequent experiments, two sets of samples without TiC were selected for the oxidation test.
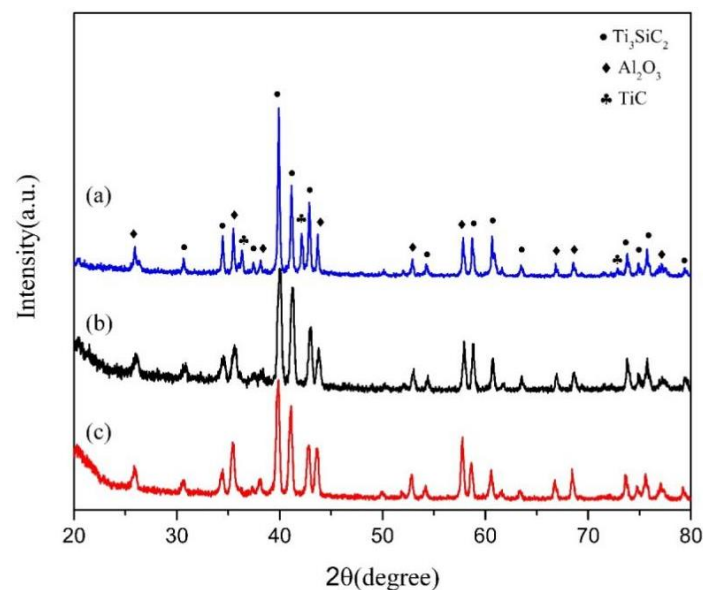

Figure 1. X-ray diffraction patterns of non-oxidizing materials: (a) TSC70, (b) TSC60 and (c) TSC50.

Figures 2 and 3 show the XRD patterns of the TSC50 and TSC60 samples, respectively, oxidized at 1400 °C. After the oxidation of TSC50 for up to 4 h, XRD showed that the TiO_2 content was relatively low. The presence of matrix Ti_3SiC_2 and Al_2O_3 was caused by the short oxidation time, and a dense and continuous oxide layer was not formed. Thus, the exposure of the matrix to the surface was accompanied by a small amount of TiO_2. In contrast to TSC50, the oxidation products of TSC60 with less Al_2O_3 were different after 4 h of oxidation. The intensity of the Ti_3SiC_2 peaks in TSC60 were significantly reduced, and the oxidized surface was mainly composed of TiO_2, Al_2O_3, and newly generated Al_2TiO_5, indicating that a continuous and thin oxide layer was formed on the sample surface.
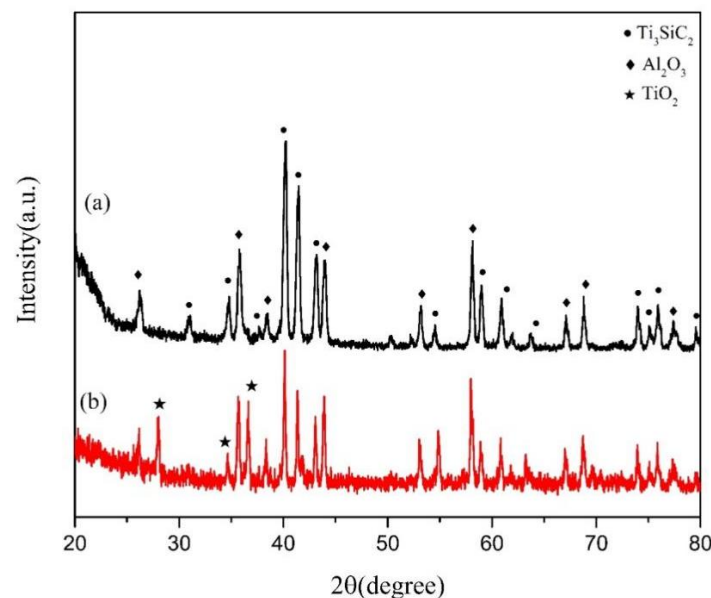

Figure 2. X-ray diffraction patterns of the TSC50 (a) before oxidation and (b) after oxidation at 1400 °C for 4 h.
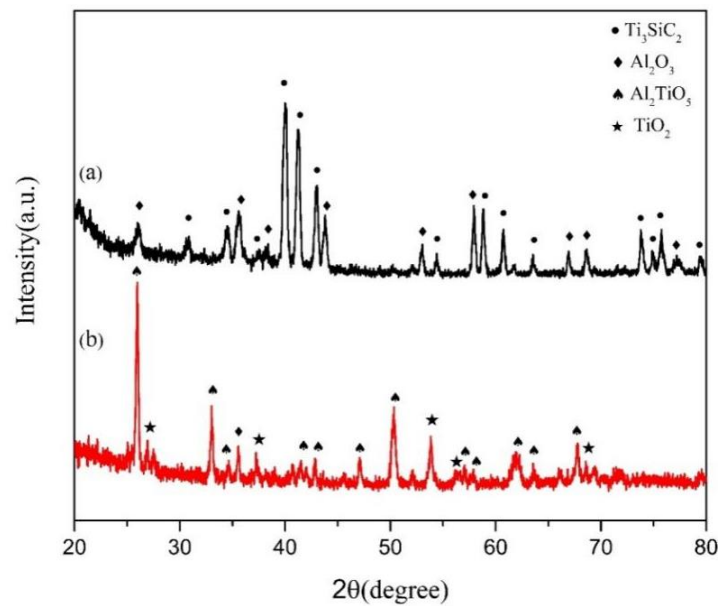
Figure 3. X-ray diffraction patterns of the TSC60 (a) before oxidation and (b) after oxidation at 1400 °C for 4 h.

As shown in Figure 4, the scanning electron microscopy (SEM) results show the surface morphology of the oxide layer after the oxidation of TSC50 and TSC60 for 4 h. Ti_3SiC_2 and Al_2O_3 remained on the surface of the TSC50 oxide layer. The morphology of the grains was massive and layered, and the pores were clearly observed. After oxidation, some grains were aggregated, which indicates oxide layer growth. The newly generated TiO_2 was connected to Ti_3SiC_2 with an evident layered structure, indicating its tendency to encapsulate Ti_3SiC_2. Conversely, after the oxidation of TSC60, the grain morphology on the oxide layer surface did not exhibit a lamellar structure. Although the grain size on the oxide layer surface of TSC60 was larger than that of TSC50, the grain morphology of TSC50 was more regular with a more distinct orientation. Stomata were observed on the surface of TSC50, and these pores may serve as channels for oxygen diffusion into the matrix. Compared with the sparsely oxidized surface of TSC50, TSC60 exhibited a state of mutual fusion and airtightness among the grains. Moreover, the fusion boundary of TSC60 could be clearly observed. Trace pores and cracks were observed on the oxidized surface of TSC60. The cause of the cracks may be the short oxidation time and the incomplete growth of the oxide layer. The difference in the oxidized surface morphology may be owing to the variation in the Al_2O_3 contents, which causes different degrees of oxidation between oxygen and Ti_3SiC_2 during the oxidation process.
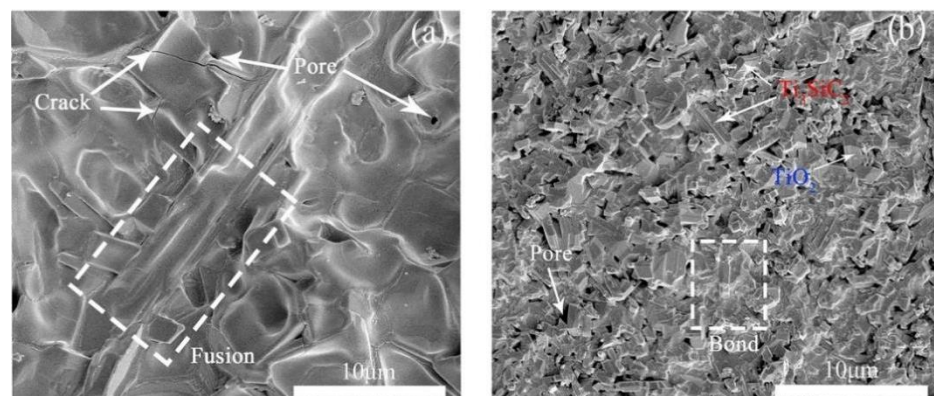

Figure 4. Surface morphology of the oxide layer after oxidation of (**a**) TSC60 and (**b**) TSC50 at 1400 °C for 4 h.

Figures 5 and 6 show the surface morphology and energy dispersive X-ray spectroscopy (EDS) results of TSC50 and TSC60 after 4h of oxidation. The oxidized surface formed a well-shaped crystal. EDS analysis indicated that the dense massive crystals on the oxidized surface of TSC50 (Figure 5) mainly contained Ti, Al, and O. Based on the types of elements and grain structures observed, the main components observed at points 1 and 2 in Figure 5 were identified as Al_2O_3 and TiO_2. Moreover, Si was not detected, indicating that SiO_2 was not present on the oxidized surface. Furthermore, a minor difference in the contents of Ti and Al was observed. Additionally, Figure 6 shows two types of crystal morphologies, in which the content of Al (the flat grain identified by point 1) was much higher than that of Ti. Based on the XRD results, the oxidized surface of TSC60 contained a small amount of Al_2TiO_5. Aluminium titanate has a plate-titanite-type crystal morphology with typical plate-like and blade-like crystals. Therefore, the grain indicated at point 1 in Figure 6 is proposed to be Al_2TiO_5. Simultaneously, the grain indicated at point 2 had a higher content of elemental Ti and appeared columnar, which is consistent with the crystal structure of rutile. Therefore, the EDS results were in good agreement with the XRD results.
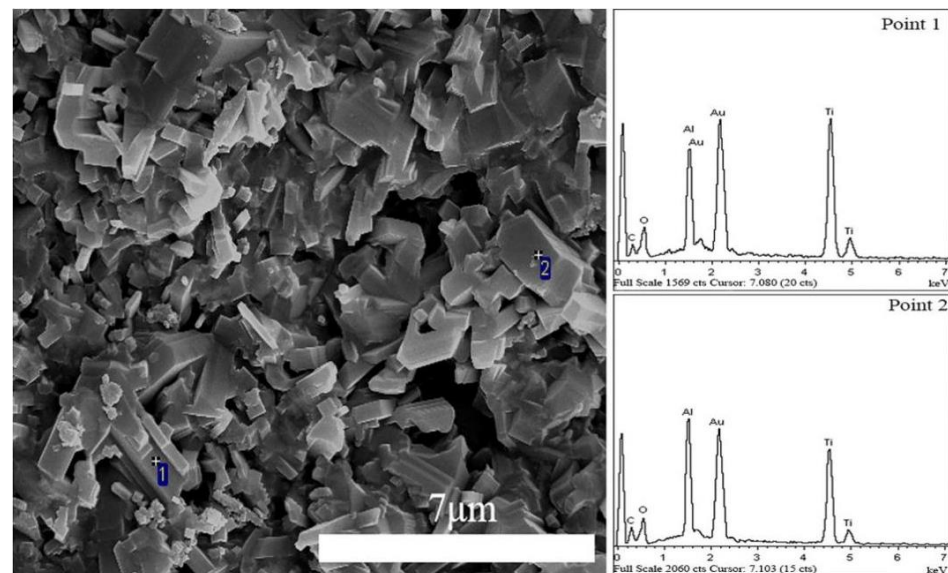

Figure 5. EDS analysis of TSC50 after oxidation at 1400 °C for 4 h.
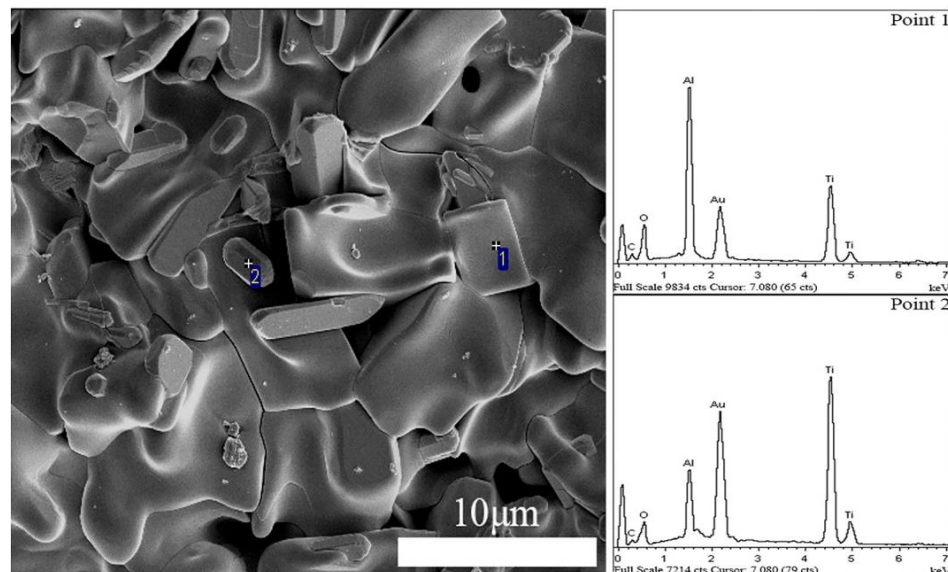

Figure 6. EDS analysis of TSC60 after oxidation at 1400 °C for 4 h.

Figure 7 shows the change in the weight gain per unit area of the two composites over time at a temperature of 1400 °C. During the oxidation period of 0–4 h, the weight gain per unit area decreased with the increasing Al_2O_3 content in the composites. However, when the oxidation time exceeded 4 h, the weight gain per unit area increased with the increasing Al_2O_3 content. With increasing time, the weight gain of TSC60 stabilized, indicating that TSC60 had transformed after 4 h of oxidation, thus reducing the degree of the subsequent oxidation processes. After 20 h of oxidation, the weight gain of TSC50 was 42.253×10^{-3} kg/m^2, whereas that of TSC60 was 29.411×10^{-3} kg/m^2, which is approximately 70% of the former. According to the XRD and EDS results, a mixed layer of Al_2TiO_5 and TiO_2 formed on the surface of TSC60 after 4 h of oxidation. Therefore, it is proposed that the presence of a mixed layer effectively reduces the rate of the subsequent oxidation of the composites. As a material with good thermal shock resistance and excellent high-temperature stability, Al_2TiO_5 played a significant role in reducing the oxidation rate of Ti_3SiC_2/Al_2O_3 in this study.
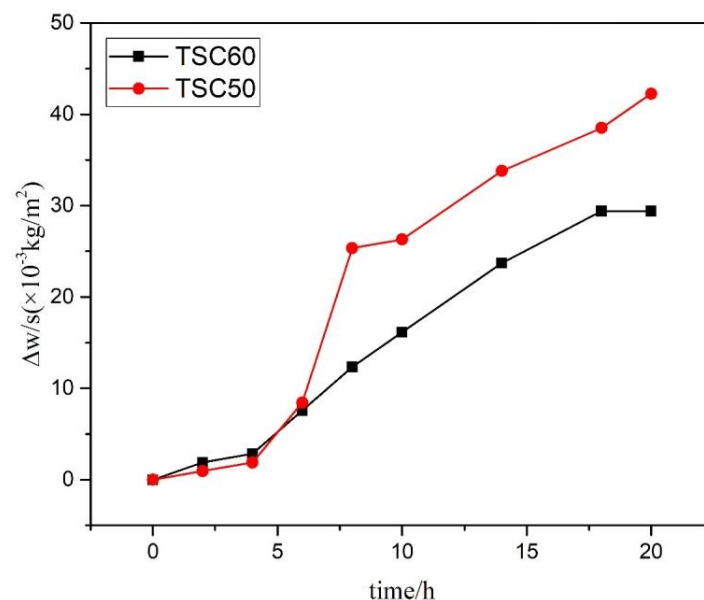

Figure 7. Weight gain per unit area of TSC50 and TSC60 at 1400 °C for 20 h.

As discussed, pores and cracks were present on the oxidized surface of Ti_3SiC_2/Al_2O_3, providing a diffusion channel for oxygen. Therefore, the oxidation of Ti_3SiC_2/Al_2O_3 was a diffusion-controlled process. Moreover, the oxidation of Ti_3SiC_2 was caused by the outward diffusion of Ti, Si and carbon, and the inward diffusion of oxygen. Although the oxidation of Ti_3SiC_2/Al_2O_3 was a diffusion-controlled process, the addition of Al_2O_3 changed the composition of the oxide layer. The cross-section of the oxide layer after 20 h of oxidation is shown in Figure 8. The thickness of the oxide layer of TSC60 was approximately 253 μm. Moreover, the oxide layer exhibited a silicone-free outer layer of approximately 40 μm. Based on the EDS results, the outer layers were clearly composed of Al_2TiO_5 and TiO_2. The presence of Si in the composite layer was detected, indicating that Si did not undergo external diffusion when it reached the composite layer, as shown in Figure 9. Thus, SiO_2 formed by silicon diffusion, and Al_2TiO_5 and Al_2O_3 compounded to form a glass phase, which increased the compactness of the composite layer and prevented the diffusion of Si and Ti [26]. As shown in Figure 9, a large amount of TiO_2 was present in the Al-deficient layer. Because the oxygen pressure in the outer layer was higher than that in the inner layer, Si gave priority to SiO gas generation. As the diffusion process progressed, SiO gas became a SiO_2 barrier that encapsulated TiO_2, resulting in a condition of Si enrichment; therefore, only a small amount of Al was detected [27]. In contrast, TSC50 did not have dense layers but it also had an Al-deficient layer of approximately 18 μm (Figure 10). At

elevated temperatures and extended periods, such as 1400 °C and 20 h, the oxidation rate was high. Notably, this temperature is similar to the melting point of Si; thus, Si was more reactive. The Si content may be one of the reasons for the difference between the TSC60 and TSC50 oxide layers. Owing to its excellent high-temperature stability, Al_2O_3 did not decompose at this oxidation temperature; however, it reacted with other oxides to protect the matrix.
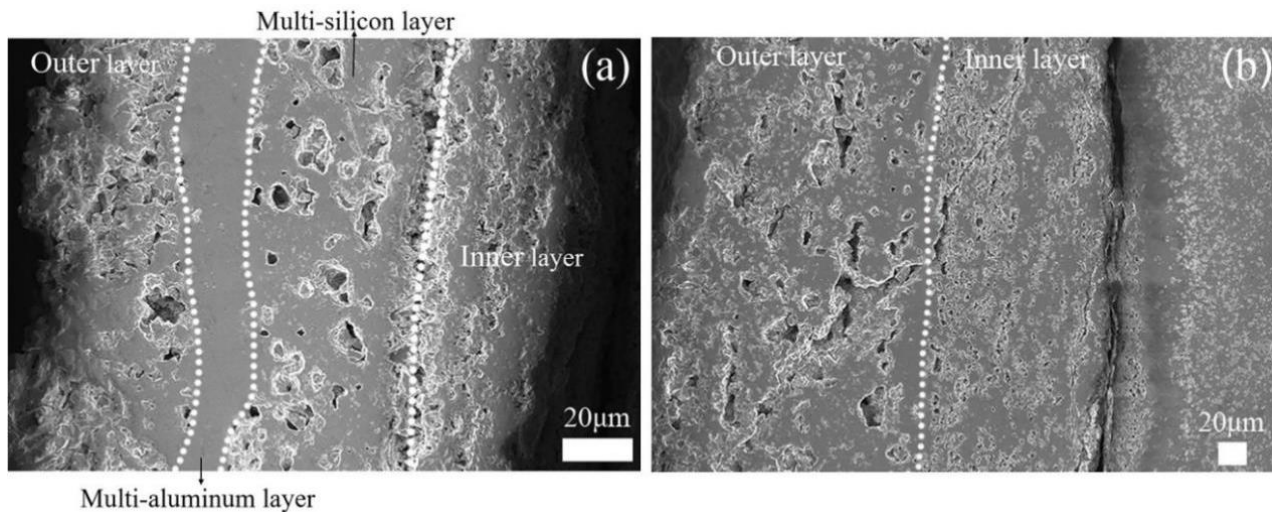

Figure 8. Cross-section of the oxide layer after oxidation of (**a**) TSC60 and (**b**) TSC50 at 1400 °C for 20 h.
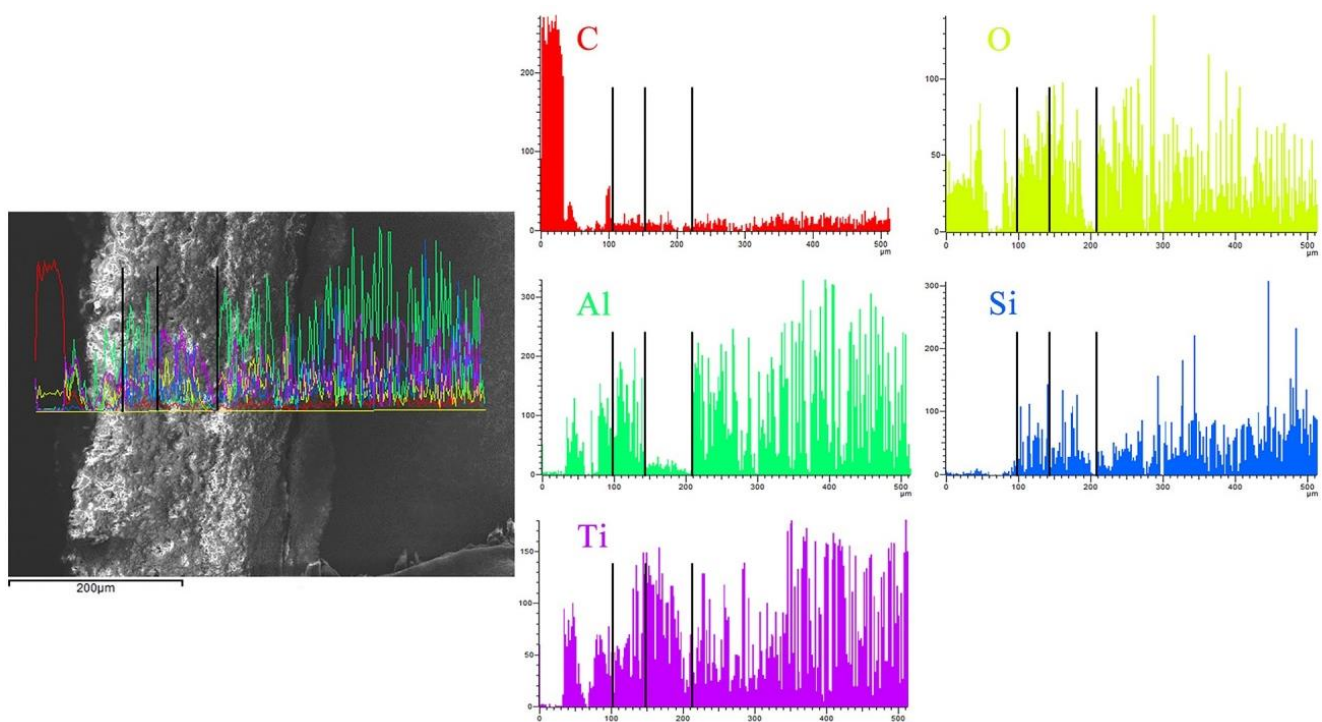

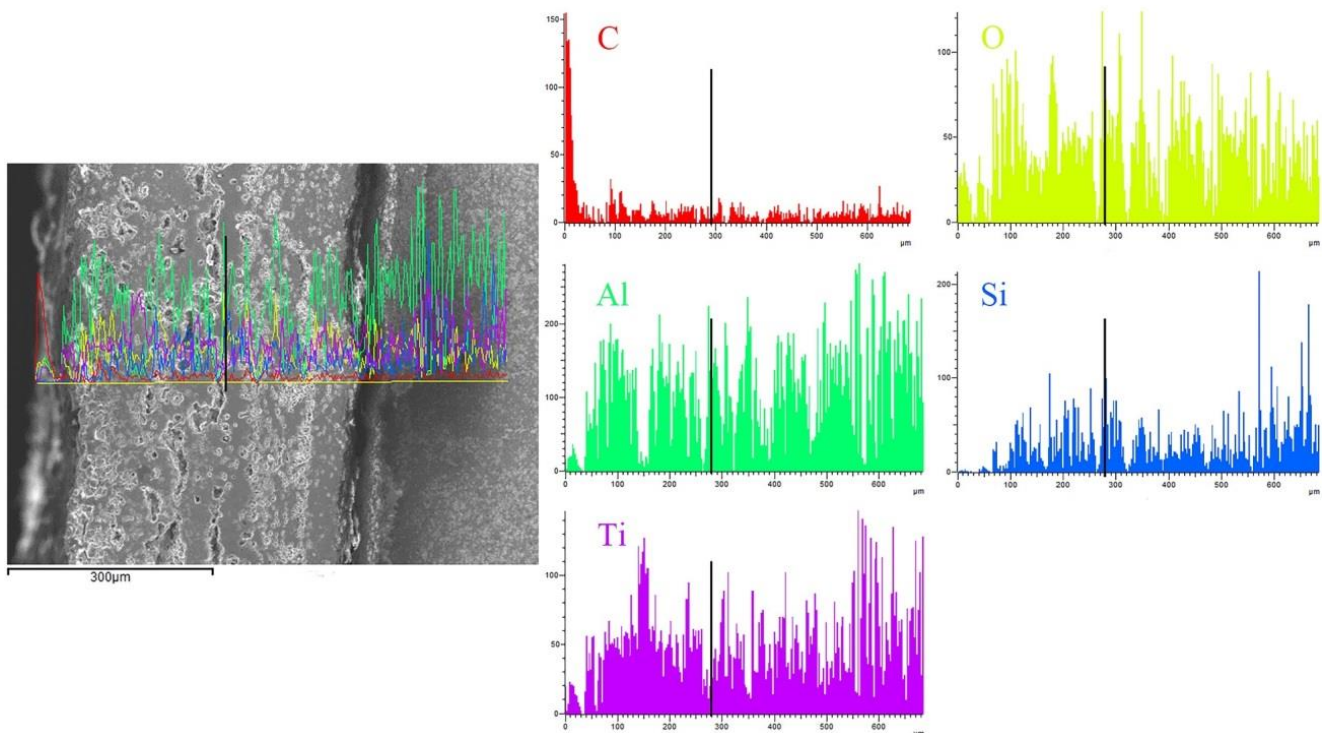**Figure 9.** EDS line scanning results of TSC60 after oxidation at 1400 °C for 20 h.

Figure 10. EDS line scanning results of TSC50 after oxidation at 1400 °C for 20 h.

Based on the above analysis, it is evident that Al_2O_3 improves the high-temperature oxidation resistance of Ti_3SiC_2. Compared with the studies reported by Zhang et al. [28] and Gao et al. [29], the oxide layer of Ti_3SiC_2/Al_2O_3 formed in this study was thinner. Moreover, the Al_2O_3 content was one of the factors influencing the oxidation resistance of the composite. Increasing the Al_2O_3 content did not always yield positive results. Thus, it is proposed that an optimal range of Al_2O_3 content exists, in which the high-temperature oxidation resistance of Ti_3SiC_2/Al_2O_3 is improved. This aspect will be investigated further in future research studies.

4. Conclusions

The compositional morphology and oxidation kinetics of Ti_3SiC_2/Al_2O_3 composites at 1400 °C were investigated in this study. The weight gain of the composite decreased with an increase in the volumetric content of Al_2O_3, indicating that Al_2O_3 addition delays the oxidation of the composite. However, when the oxidation time exceeded 4 h and continued until 20 h, the oxidation process accelerated, indicating that 4 h was the limit for the oxidation stability of the composite. After 4 h of oxidation, at 1400 °C, the surface of the composite with a high volume of Al_2O_3 exhibited more pores, facilitating the diffusion of oxygen into the matrix, which may have caused the acceleration of the oxidation process of the composites during extended periods of oxidation. The presence of Al_2TiO_5 on the oxidation surface of the composite with a low volume of Al_2O_3 may have reduced the rate of matrix oxidation and hindered the oxidation instability of the composites. Moreover, the composite oxide layer inhibited the diffusion-controlled process.

Institutional Review Board Statement: Not applicable.

Informed Consent Statement: Not applicable.

Data Availability Statement: Not applicable.

Conflicts of Interest: No conflict of interest exits in the submission of this manuscript, and the manuscript was approved by all authors for publication. I would like to declare on behalf of my co-authors that the work described was original research that has not been published previously, and is not under consideration for publication elsewhere, in whole or in part. All the authors listed have approved the manuscript that is enclosed.

References

1. Sun, Z.M. Progress in research and development on MAX phases: A family of layered ternary compounds. *Int. Mater. Rev.* **2011**, *56*, 143–166. [CrossRef]
2. Atazadeh, N.; Heydari, M.S.; Baharvandi, H.R.; Ehsani, N. Reviewing the effects of different additives on the synthesis of the Ti_3SiC_2 MAX phase by mechanical alloying technique. *Int. J. Refract. Met. Hard Mater.* **2016**, *61*, 67–78. [CrossRef]
3. Qin, J.; He, D. Phase stability of Ti_3SiC_2 at high pressure and high temperature. *Ceram. Int.* **2013**, *39*, 9361–9367. [CrossRef]
4. Dezellus, O.; Gardiola, B.; Andrieux, J.; Lay, S. Experimental evidence of copper insertion in a crystallographic structure of Ti_3SiC_2 MAX phase. *Scr. Mater.* **2015**, *104*, 17–20. [CrossRef]
5. Islak, B.Y.; Ayas, E. Evaluation of properties of spark plasma sintered Ti_3SiC_2 and Ti_3SiC_2/SiC composites. *Ceram. Int.* **2019**, *45*, 12297–12306. [CrossRef]
6. Liu, X.; Zhang, H.; Jiang, Y.; He, Y. Characterization and application of porous Ti_3SiC_2 ceramic prepared through reactive synthesis. *Mater. Des.* **2015**, *79*, 94–98. [CrossRef]
7. El Saeed, M.A.; Deorsola, F.A.; Rashad, R.M. Optimization of the Ti_3SiC_2 MAX phase synthesis. *Int. J. Refract. Met. Hard Mater.* **2012**, *35*, 127–131. [CrossRef]
8. Cai, Y.Z.; Cheng, L.F. Effect of positioning impregnation on the oxidation behaviour of Ti_3SiC_2/SiC functionally graded materials at 1400 °C. *J. Alloy. Compd.* **2018**, *742*, 180–190. [CrossRef]
9. Yang, J.S.; Zhang, X.Y. Fabrication of Ti_3SiC_2 powders using TiH_2 as the source of Ti. *Ceram. Int.* **2012**, *38*, 3509–3512. [CrossRef]
10. Zheng, L.-L.; Sun, L.-C.; Li, M.-S.; Zhou, Y.-C. Improving the high-temperature oxidation resistance of $Ti_3(SiAl)C_2$ by Nb-doping. *J. Am. Ceram. Soc.* **2011**, *94*, 3579–3586. [CrossRef]
11. Li, X.; Qian, Y.; Zheng, L.; Xu, J.; Li, M. Determination of the critical content of Al for selective oxidation of Ti_3AlC_2 at 1100 °C. *J. Eur. Ceram. Soc.* **2016**, *36*, 3311–3318. [CrossRef]
12. Li, X.; Zheng, L.; Qian, Y.; Xu, J.; Li, M. Breakaway oxidation of Ti_3AlC_2 during long-term exposure in air at 1100 °C. *Corros. Sci.* **2016**, *104*, 112–122. [CrossRef]
13. Gong, Y.; Tian, W.; Zhang, P.; Chen, J.; Zhang, Y.; Sun, Z. Slip casting and pressureless sintering of Ti_3AlC_2. *J. Adv. Ceram.* **2019**, *8*, 367–376. [CrossRef]
14. Qi, F.F.; Wang, Z. Improved mechanical properties of Al_2O_3 ceramic by in-suit generated Ti_3SiC_2 and TiC via hot pressing sintering. *Ceram. Int.* **2017**, *43*, 10691–10697. [CrossRef]
15. Shi, S.L.; Pan, W. Toughening of Ti_3SiC_2 with 3Y-TZP addition by spark plasma sintering. *Mater. Sci. Eng. A* **2007**, *447*, 303–306. [CrossRef]
16. Islak, B.Y.; Candar, D. Synthesis and properties of TiB_2/Ti_3SiC_2 composites. *Ceram. Int.* **2021**, *47*, 1439–1446. [CrossRef]
17. Zhang, J.; Wang, L.; Jiang, W.; Chen, L. High temperature oxidation behavior and mechanism of Ti_3SiC_2-SiC nanocomposites in air. *Compos. Sci. Technol.* **2008**, *68*, 1531–1538. [CrossRef]
18. Li, S.; Song, G.M.; Zhou, Y. A dense and fine-grained SiC/$Ti_3Si(Al)C_2$ composite and its high-temperature oxidation behavior. *J. Eur. Ceram. Soc.* **2012**, *32*, 3435–3444. [CrossRef]
19. Xu, X.; Ngai, T.L.; Li, Y. Synthesis and characterization of quarternary $Ti_3Si_{(1-x)}Al_xC_2$ MAX phase materials. *Ceram. Int.* **2015**, *41*, 7626–7631. [CrossRef]
20. Guedouar, B.; Hadji, Y. Oxidation behavior of Al-doped Ti_3SiC_2-20wt.%Ti_5Si_3 composite. *Ceram. Int.* **2021**, *47*, 33622–33631. [CrossRef]
21. Heider, B.; Scharifi, E.; Engler, T.; Oechsner, M.; Steinhoff, K. Influence of heated forming tools on corrosion behavior of high strength aluminum alloys. *Mater. Sci. Eng. Technol.* **2021**, *52*, 145–151. [CrossRef]

22. Popov, A.I.; Lushchik, A.; Shablonin, E.; Vasil'chenko, E.; Kotomin, E.A.; Moskina, A.M.; Kuzovkov, V.N. Comparison of the F-type center thermal annealing in heavy-ion and neutron irradiated Al_2O_3 single crystals. *Nucl. Instrum. Methods Phys. Res. Sect. B Beam Interact. Mater. At.* **2018**, *433*, 93–97. [CrossRef]

23. Averback, R.S.; Ehrhart, P.; Popov, A.I. Defects in ion implanted and electron irradiated Mgo and Al_2O_3. *Radiat. Eff. Defects Solids* **1995**, *136*, 169–173. [CrossRef]

24. Shablonin, E.; Popov, A.I.; Prieditis, G.; Vasil'chenko, E.; Lushchik, A. Thermal annealing and transformation of dimer F centers in neutron-irradiated Al_2O_3 single crystals. *J. Nucl. Mater.* **2021**, *543*, 152600. [CrossRef]

25. Sun, Z.; Zhou, Y.; Li, M. High temperature oxidation behavior of Ti_3SiC_2-based material in air. *Acta Mater.* **2001**, *49*, 4347–4353. [CrossRef]

26. Dong, X.; Wang, Y.; Wang, R.; Wang, X.; Li, Y. Study on Al_2TiO_5-SiO_2-Al_2O_3 composites. *Bull. Chin. Ceram. Soc.* **2008**, *27*, 649–653.

27. Zhang, H.B.; Shen, S.Y. Oxidation behavior of porous Ti_3SiC_2 prepared by reactive synthesis. *Trans. Nonferrous Met. Soc. China* **2018**, *28*, 1774–1783. [CrossRef]

28. Zhang, H.B.; Zhou, Y.C.; Bao, Y.W.; Li, M.S. Improving the oxidation resistance of Ti_3SiC_2 by forming a $Ti_3Si_{0.9}Al_{0.1}C_2$ solid solution. *Acta Mater.* **2004**, *52*, 3631–3637. [CrossRef]

29. Gao, H.; Benitez, R.; Son, W.; Arroyave, R.; Radovic, M. Structural, physical and mechanical properties of $Ti_3(Al_{1-x}Si_x)C_2$ solid solution with x = 0–1. *Mater. Sci. Eng. A* **2016**, *676*, 197–208. [CrossRef]